Modeling and simulation of viscoelastic solids under large numbers of loading cycles

Article *in* Mechanics of Advanced Materials and Structures · February 2022

DOI: 10.1080/15376494.2022.2037170

3 authors:

Darith Hun
Catholic University of Louvain
10 PUBLICATIONS **58** CITATIONS
SEE PROFILE

Mohamed Haddad
Catholic University of Louvain
4 PUBLICATIONS **10** CITATIONS
SEE PROFILE

Issam Doghri
Catholic University of Louvain
126 PUBLICATIONS **5,576** CITATIONS
SEE PROFILE

Modeling and simulation of viscoelastic solids under large numbers of loading cycles

Darith Anthony Hun[a] , Mohamed Haddad[a], Issam Doghri[a]

[a] Université catholique de Louvain, Institute of Mechanics, Materials and Civil Engineering, Louvain-La-Neuve B-1348, Belgium.

ARTICLE HISTORY
Compiled January 30, 2022

ABSTRACT
An efficient modeling procedure is proposed for viscoelastic (VE) solids subjected to large numbers of loading cycles. While the Laplace-Carson transform (LCT) is often used to solve VE creep or relaxation problems, the originality here is an efficient extension of the approach to a plethora of cycles, based on some key ingredients. The time history of the cyclic loading is decomposed into transient and periodic signals, leading to two subproblems. Each one is transformed into a finite number of linear elastic analyses in the L-C domain. A method to choose the number and positioning of the L-C domain sampling points for each one of the two subproblems is detailed. Specific LCT inversion methods are applied to each subproblem in order to reconstruct the displacement, strain and stress fields in the time domain. For the transient subproblem, Schapery's collocation method based on exponential basis functions is used, while a new LCT inversion method is proposed for the periodic subproblem based on sinusoidal basis functions and a Newton-Gauss algorithm. After a verification on well-known 1D functions, the accuracy of the proposed method is assessed on two structural problems with large numbers of cycles. Comparison with reference finite element analyses conducted directly in the time domain shows that the proposed methodology provides excellent predictions, both at local scale (displacement, strain and stress components at various points) and macroscale (global energy indicator). The important speedup factor (e.g., 32 for 10k cycles) will increase significantly with the number of cycles, enabling the proposed method to be extended to high cycle fatigue of thermoplastic polymer structures in future work.

KEYWORDS
Laplace-Carson numerical inversion, high cycle simulation, periodic basis extension, viscoelastic structure.

1. Introduction

Numerical simulation of high cycle fatigue for structures whose material behavior remains inelastic and dissipative through the cyclic history is an important challenge, in particular for thermoplastic polymer structures. The latter are increasingly used especially with the emergence and improvement of different additive manufacturing technologies [1, 2], which allow the user to design the geometry and/or the mechanical performance of the structure. However, in the long-term and under repeated loading these structures weaken and may even fail. Proposing a model that can accurately predict these phenomena while taking into account the intrinsic behavior of the medium represents a great interest for mechanical engineering. In the literature, many constitutive models and numerical algorithms about the thermomechanical behavior of these thermoplastic polymer materials have been developed. A ViscoElastic-ViscoPlastic model (VE-VP) [3, 4] has been often selected because it allows a flexibility of responses in both the ViscoElastic (VE) and ViscoPlastic (VP) regimes. Extended to the framework of large numbers of cycles, Haouala and Doghri [5] propose for single volume elements under imposed strain history a method of time homogenization allowing a strong gain of computation time ($\sim 94\%$) for a small error on the stress response ($\leq 4\%$). The natural extension of this method would be an adaptation to a structural problem. Indeed, a classical finite element solution would require a prohibitive computation

CONTACT Issam Doghri. Email: issam.doghri@uclouvain.be

Mechanics of Advanced Materials and Structures (in press).

time due first to the large numbers of loading cycles and also to the solvers used to numerically manage the material non-linearities.

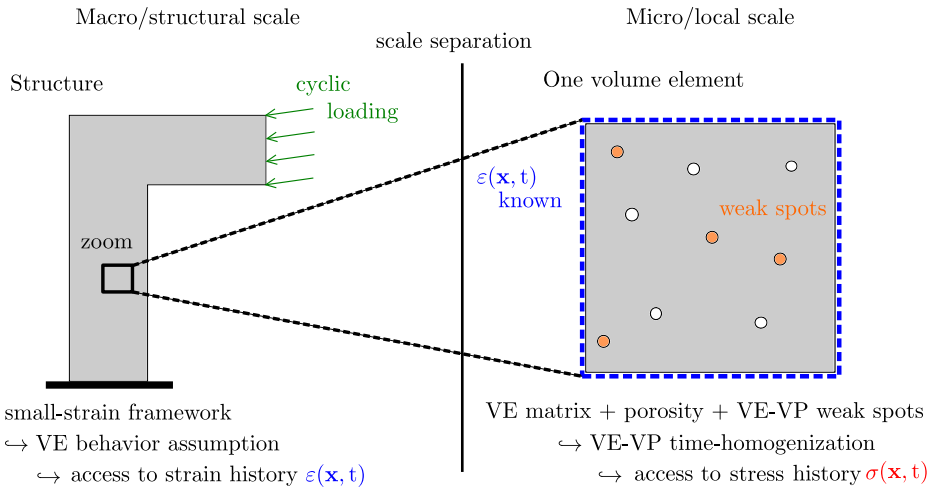

Figure 1.: Multiscale in space and time strategy proposed for structures subjected to large numbers of cycles and made of heterogeneous VE-VP thermoplastic polymer materials (see [6]).

To overcome this issue, a multiscale strategy in space and time is proposed, which is illustrated in Fig. 1. As proposed by Krairi et al. in [6], high cycle fatigue of thermoplastic polymer structures can be explained at microlevel by supposing that each representative volume element is made of a VE matrix material containing a small volume fraction ($\sim 2\%$) of VE-VP weak spots. We also consider a small ($\sim 3\%$) porosity distribution due to manufacturing process (e.g., selective laser sintering, [1, 2]). Under the hypothesis of small deformations, the idea is then in the present work to postulate that the structure will follow globally a VE deformation throughout the cyclic loading and that the plastification leading to the weakening of the structure occurs at microscale in some local regions, affecting finally only marginally the macroscopic structural response. In order to implement and validate the proposed strategy, there are two major issues which need to be addressed, and each one represents an original contribution. The first problem to overcome, located at the macroscopic scale, would be to propose a method to solve a structural VE problem at a low computational cost. Once the deformation history is obtained, the next step would be to couple this structural deformation history with the local time-homogenization method [5] applied on the real complex microstructure (modeled as VE matrix, porosity and weak spots) and to validate the whole multiscale strategy on a full reference structural computation. In this paper we focus on the first problem, the study aiming to accelerate the simulation time of VE structures under large numbers of cycles.

The cost of solving a VE time problem is dependent on the number of cycles and requires time integration schemes that must respect approximations [7] to converge to the solution. This cost becomes prohibitive for a problem with large numbers of cycles. In the literature, different numerical methods allow to reduce the calculation time. An extended PGD (Proper General Decomposition) method is presented in [8] for a VE material, under creep or cyclic loadings. Basically this method defines an approximate solution constructed on an enriched basis function. In this application, the response is compared to a reference and allows a time saving of 5 and an error lower than 3%. The jump cycle method is used in [9] for a more general material (VE-VP-damage). This method works in two steps, the first one consists in calculating a solution for a certain number of cycles and then extrapolating it temporally on a neighboring interval. The operation is then repeated until the complete history time interval is covered. In that work, the final solution is then obtained by skipping 60% of the cycles for an error around 5%. In the present article, in order to reduce the computational time for VE structures subjected to large numbers of cycles, we use another method based on the Laplace-Carson transform (LCT) and its numerical inversion. We develop some key ingredients which enable to combine an important speedup factor (much higher than with existing methods) with a very accurate reconstruction of the strain and stress fields in realistic structural problems.

The LCT of a function f is defined as follows :

$$\mathscr{L}_p\{f(t)\} = f^\star(p) = p\int_0^\infty f(t)e^{-pt}dt, \tag{1}$$

where $t \mapsto f(t)$ is a scalar or tensorial function defined in the original space and $p \mapsto f^\star(p)$ is in the L-C space.

Basically, this LCT allows to change an integral problem with a convolution product in the original space, into a simple product in the L-C space, facilitating the algebraic and/or numerical resolution. This LCT is often used in engineering, e.g, in the field of electrical engineering [10, 11] or in mechanics of materials with VE behavior [12, 13, 14]; in these two fields the original space is time. This transformation calling the correspondence principle of Lee-Mandel [15] provides a faster solution in the L-C domain. However, the inversion of the response in the time domain (Bromwich formula) :

$$\mathscr{L}_t^{-1}\{f^\star(p)\} = f(t). \tag{2}$$

is not always applicable in practice. During this step the accuracy depends directly on the response function, which for simple cases (well-known algebraic functions) can be solved analytically. For more complex functions f, numerical approximation inversion methods are then employed. Among all these numerical methods, we can reference two main families :

(1) General inversion algorithms : Abate and Whitt provide in [16] a large bibliography of these numerical methods which use general function bases, e.g. : Fourier series originally coming from [17, 18], Gaver's functional [19, 20], or Bromwich's integral [21].
(2) Specific inversion algorithms : where the inversion basis is "designed" by the shape of the f solution known *a priori*. These methods are particularly adapted to the linear VE problem which gives by construction of a constitutive model and/or boundary conditions an indication on the shape of the responses. For creep/relaxation type mechanical responses, by fixing certain parameters of their models [22, 23] proposed a direct inversion method under an exponential projection basis, particularly adapted to VE behavior where the time-evolution of material properties is described with decaying exponentials (Prony series). Indirect methods like [14, 24, 25], use optimization algorithms to reduce the error between the solution and the approximate function in the L-C domain. One of the advantages is a better accuracy compared to the direct method against an additional time cost due to the convergence of the optimizer.

In both cases, these two families of algorithms continuously define the solution function f in the time domain on the basis of the discretized solution function $f^\star$ in the L-C domain.

The method proposed in this paper belongs to the second family and applies to VE structural mechanics problems in the framework of large numbers of loading cycles. The main focus and the originality with respect to the existing literature is the accurate reconstruction in time domain of all strain components in any Gauss point of the structural FE mesh. This is achieved thanks to some key ingredients : (i) structural VE problem decomposition into two subproblems, transient and periodic; (ii) use of exponential basis functions and Schapery's collocation method for the transient subproblem; (iii) use of sinusoidal basis functions and a Gauss-Newton algorithm for the periodic subproblem; (iv) a rigorous procedure to determine the adequate number and the positioning of the sampling points in the L-C domain for each subproblem; (v) solving a limited number of structural elastic problems in the L-C domain; (vi) computationally efficient and accurate reconstruction of displacement, strain and stress fields in the time domain. The paper is organized as follows: In Section 2, two LCT inversion methods are presented in a general setting and applied on well-known 1D periodic functions (mono and multi-harmonic). In Section 3, the proposed computational procedure for VE structures subjected to large numbers of loading cycles is developed. The methodology is applied on on two different structures. A comparison between results and computational cost obtained by the proposed method and reference calculations in time domain is also shown. Conclusions are drawn is Section 4. Three appendices (A, B and C) deal with the influence of the number of sampling points, the sampling method and the computational time comparison.

2. LCT inversion methods for VE problems

In this section, we present two LCT inversion methods. The first is Schapery's collocation method used when the time function is a sum of exponentials. The shortcomings of the method are illustrated. The second method is proposed for periodic time functions expressed as a sum of sinusoids.

2.1. Schapery's collocation method

The collocation method proposed by Schapery [22] for numerical LCT inversion is still often used in VE mechanical problems. In this framework the author defined the solution f of the problem in time t as a series of exponentials such that :

$$f(t) = A + Bt + \sum_{k=1}^{N} b_k(1 - e^{-t/\theta_k}), \tag{3}$$

This decomposition is parametrized by the set (b_k,θ_k), A and B are shift parameters. This decomposition is adapted to represent both the classical phenomena of creep ($\theta_k < 0$) and relaxation ($\theta_k > 0$) related to a VE behavior.
This decomposition in time of the f solution has its analogous form $f^\star$ in the L-C domain by successive transformation of each term such that :

$$f^\star(p) = A + \frac{B}{p} + \sum_{k=1}^{N} b_k \frac{1}{1 + p\theta_k}. \tag{4}$$

The A and B parameters are evaluated with the limit values in time or (in practice) in L-C domain as :

$$A = \lim_{t\to 0} f(t) = \lim_{p\to +\infty} f^\star(p), \tag{5}$$

$$B = \lim_{t\to +\infty} \frac{f(t)}{t} = \lim_{p\to 0} pf^\star(p). \tag{6}$$

The LCT solution function $f^\star$ is then estimated on several discrete points $p_i (i \in \{1, ..., M\}$, M the number of discrete points) allowing the identification of the set (b_k,θ_k) and the reconstruction of a reference function $f(t)$ in the time domain. Based on the discretization of Eq. 4, and using the constraint : $\theta_i = 1/p_i$, the system is reduced to computing b_k parameters only. The coefficients are identified by solving the following linear system :

$$\begin{Bmatrix} b_1 \\ b_2 \\ b_3 \\ \vdots \\ b_N \end{Bmatrix} = \begin{bmatrix} \frac{1}{1+p_1/p_1} & \frac{1}{1+p_1/p_2} & \frac{1}{1+p_1/p_3} & \cdots & \frac{1}{1+p_1/p_N} \\ \frac{1}{1+p_2/p_1} & \frac{1}{1+p_2/p_2} & \frac{1}{1+p_2/p_3} & \cdots & \frac{1}{1+p_2/p_N} \\ \frac{1}{1+p_3/p_1} & \frac{1}{1+p_3/p_2} & \frac{1}{1+p_3/p_3} & \cdots & \frac{1}{1+p_3/p_N} \\ \vdots & \vdots & \vdots & \ddots & \vdots \\ \frac{1}{1+p_N/p_1} & \frac{1}{1+p_N/p_2} & \frac{1}{1+p_N/p_3} & \cdots & \frac{1}{1+p_N/p_N} \end{bmatrix}^{-1} \begin{Bmatrix} f^\star(p_1) - (A + B/p_1) \\ f^\star(p_2) - (A + B/p_2) \\ f^\star(p_3) - (A + B/p_3) \\ \vdots \\ f^\star(p_N) - (A + B/p_N) \end{Bmatrix}. \tag{7}$$

It should be noted that the order N of the series and the number M of discrete points p_i are dependent on each other ($N = M$) to ensure a well-posed system. The advantage of this method lies in a direct numerical solution and an easy implementation. Theoretically, once the system is solved and all parameters b_k are identified, $f(t)$ can be reconstructed at any time. However, in practice, the accuracy of the reconstruction strongly depends on the number of sample points p_i, as illustrated in Fig. 2.

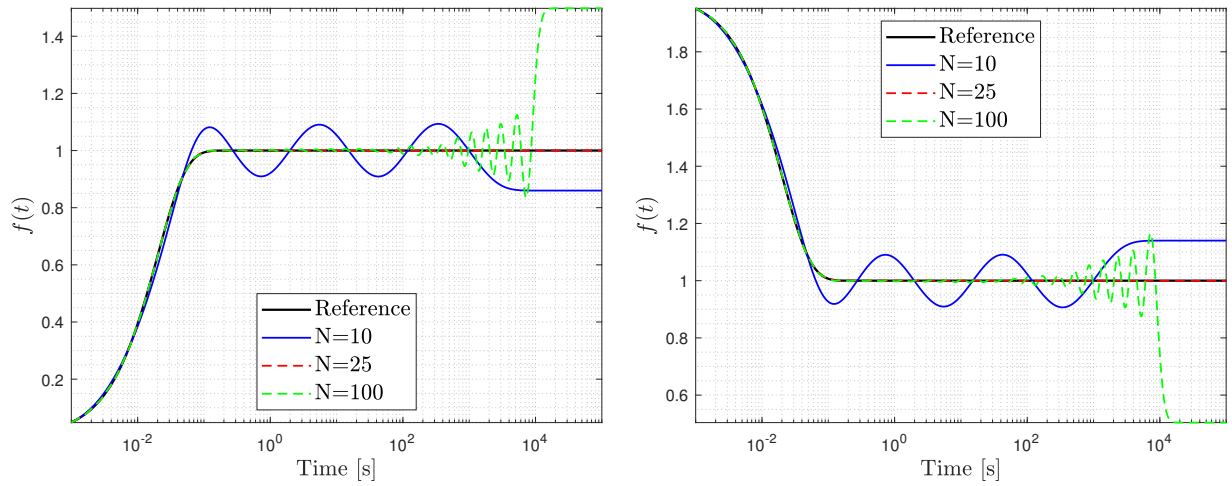

(a) Creep test. (b) Relaxation test.

Figure 2.: Effect of number of collocation points (under-sampling and over-sampling) on the accuracy of Schapery's method.

In this illustrative example the reference time function $\widetilde{f}(t)$ to be recovered is :

$$\widetilde{f}(t) = 1 + Ce^{-t/\theta}, \tag{8}$$

representing the shape of the response under relaxation ($C = 1$, see Fig. 2b) or creep test ($C = -1$, see Fig. 2a) and $\theta = 0.02s$, the relaxation time. In these illustrations, a low number of points (N = 10) does not allow to capture enough information to represent the solution and an oversampling (N = 100) increases the size of the system and its singularity, thus adding parasitic oscillations to the original solution in time, as reported in [13]. In practice and in this example, a short preliminary study was conducted and a choice of $N = 25$ points p_i equally positioned on a logarithmic scale allows to recover the solution correctly.

2.2. Proposed LCT inversion method for sinusoidal functions

Schapery used an exponential projection basis to approximately reconstruct a time function, particularly well adapted for creep and relaxation response. However, for a cyclic structural simulation, our goal is to accurately reconstruct the time histories of the strain components $\varepsilon_{ij}(\mathbf{x}, t)$ at various positions $\mathbf{x}$ of a structure subjected to cyclic loading. In this context, it is more pertinent to consider a decomposition built on a sinusoidal basis, which is described in time as :

$$f(t) = \sum_{k=1}^{N} a_k \sin(\omega_k t + \phi_k), \tag{9}$$

with the set $\mathbf{A_k} = (a_k,\omega_k,\phi_k)$ of parameters to be identified, which are respectively the amplitude, the pulsation and the shift of the approached function. The analogous form in L-C domain of this projection basis is defined as :

$$f^{\star}(p) = \sum_{k=1}^{N} \left\{ a_k \frac{p^2}{\omega_k^2 + p^2} \sin(\phi_k) + a_k \frac{\omega_k p}{\omega_k^2 + p^2} \cos(\phi_k) \right\}. \tag{10}$$

The solution function $f^{\star}$ is then estimated on several discrete points p_i and an algorithm allows the identification of the set $\mathbf{A_k}$ and the reconstruction in the time domain.
For this example, an optimization algorithm was selected, as in [14, 24, 25], namely the Gauss-Newton algorithm. This choice was motivated by the use of a tangent operator (additional constraint on the first

derivatives) which can be defined analytically on the basis of projection in the L-C domain and allowing the convergence as well as the elimination of spurious higher modes generated by oversampling. It is an iterative method, well-known and general. The algorithm is explained and applied in the present case on the periodic projection basis and the (3xN)-parameters are identified using this following vector form :

$$\begin{Bmatrix} \mathbf{a} \\ \boldsymbol{\omega} \\ \boldsymbol{\phi} \end{Bmatrix}^{\text{new}}_{(3\times\text{N},1)} = \begin{Bmatrix} \mathbf{a} \\ \boldsymbol{\omega} \\ \boldsymbol{\phi} \end{Bmatrix}^{\text{old}}_{(3\times\text{N},1)} + \begin{Bmatrix} \boldsymbol{\Delta a} \\ \boldsymbol{\Delta\omega} \\ \boldsymbol{\Delta\phi} \end{Bmatrix}_{(3\times\text{N},1)}, \tag{11}$$

or :

$$\{\mathbf{A}\}^{\mathbf{new}} = \{\mathbf{A}\}^{\mathbf{old}} + \{\mathbf{\Delta A}\}, \tag{12}$$

where $\{\mathbf{A}\}=(\mathbf{a},\boldsymbol{\omega},\boldsymbol{\phi})^T$ is a (3xN) size vector containing respectively all the set of $\mathbf{A_k}$ parameters, and $\mathbf{\Delta A}$ is the correction vector of the Newton-Gauss algorithm defined classically as :

$$\{\mathbf{\Delta A}\}_{(\mathbf{3\times N,1})} = \left[[-\mathbf{J^T J}]^{-\mathbf{1}}\mathbf{J^T}\right]_{(\mathbf{3\times N,M})} \{\mathbf{r}\}_{(\mathbf{M\times 1})} \tag{13}$$

where $\{\mathbf{r}\}$ is the residual error vector containing $r_i = \widetilde{f^\star}(p_i) - f^\star(p_i,\mathbf{A})$ component, $[\mathbf{J}]$ is the (M,3xN) Jacobian matrix (not necessarily square) written as :

$$[\boldsymbol{J}]_{(M,3\text{x}N)} = \left[[\boldsymbol{J_a}]_{(M,N)}, [\boldsymbol{J_\omega}]_{(M,N)}, [\boldsymbol{J_\phi}]_{(M,N)}\right] \tag{14}$$

and defined as the derivative of the residuum error vector and parameters

$$[J_a]_{ik} = -\frac{\partial f_i^\star}{\partial a_k},\ [J_\omega]_{ik} = -\frac{\partial f_i^\star}{\partial \omega_k},\ [J_\phi]_{ik} = -\frac{\partial f_i^\star}{\partial \phi_k}. \tag{15}$$

Where $f_i^\star = f^\star(p_i;\mathbf{A})$ is the discretized $f^\star$ with $\mathbf{A}$ coefficients to identified and $\widetilde{f^\star}$ the function to recover. It should be noted that on the basis of the sinusoidal decomposition used, the system requires a discrete number of points M≤3xN, the oversampling does not affect the accuracy of the projected solution.

A first illustration of this LCT inversion method is proposed on a unimodal periodic signal (N=1) in Fig. 3b, where the reference solution to be recovered (in black curve) is written as :

$$\widetilde{f}(t) = a\sin(\omega t + \phi) \tag{16}$$

and its LCT analogous form as :

$$\widetilde{f^\star}(p) = a\frac{p^2}{\omega^2+p^2}\sin(\phi) + a\frac{\omega p}{\omega^2+p^2}\cos(\phi), \tag{17}$$

with ($a=1$, $\omega=2$, $\phi=\pi/6$).

This reference function $\widetilde{f}$ (in black) is compared first to Schapery's collocation method (in blue), where the numerical approached solution and the exponential basis used have been described in Eq. 3 & 4, with N = 60 discrete points (p_i), and then the proposed method (in red), where the reconstructed solution is approached by a sinus basis and computed by an optimization algorithm described in Eq. 13 & 14, with the starting coefficients ($a_1^{(0)} = 0.8\times a$, $\omega_1^{(0)} = 1\times\omega$, $\phi_1^{(0)} = 2\times\phi$), for N = 30 discrete points.

Fig. 3b shows that in order to reconstruct the sinusoidal function of Eq. 16, the proposed method needs only 30 sampling points to yield a very accurate reconstruction. However, on the same example, Schapery's collocation method needs twice as many points (60) and nevertheless loses accuracy after two cycles. An extended study of the accuracy of the two methods in the reconstruction of the sinusoidal

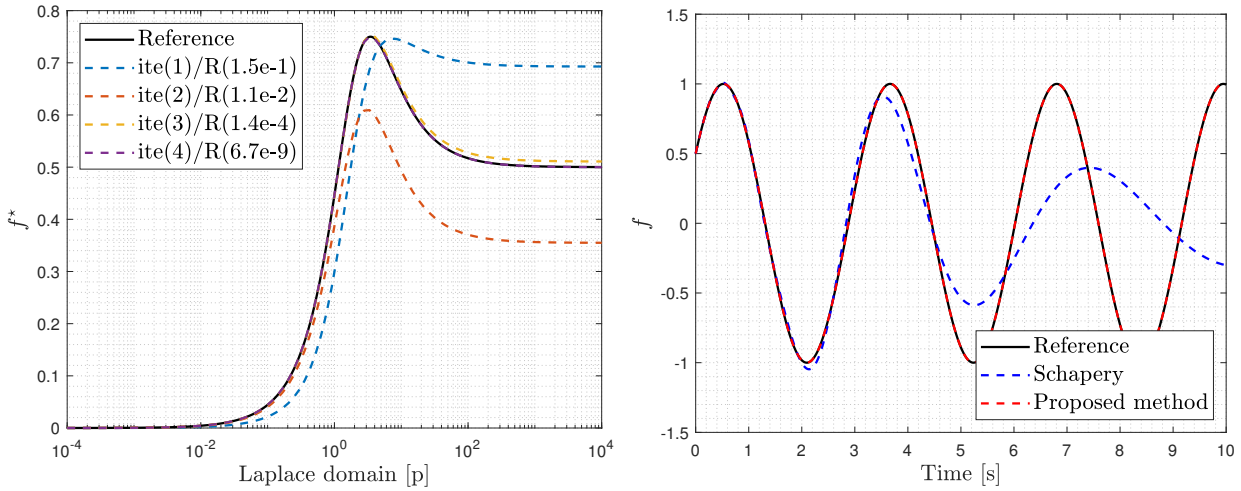

(a) Convergence of the residue and the iterative approached solutions associated with the reference solution in L-C domain.

(b) Comparison of two approximate reconstructions with the reference solution in time domain.

Figure 3.: Accuracy of the proposed LCT inversion for a sinusoidal function.

reference solution depending on the number of sampling points is provided in Appendix A. With this parametrization, the iterative convergence of the LCT (see Eq. 10) with the $\mathbf{A}$ vector to be identified in L-C domain is shown in Fig. 3a. We have defined the residuum indicator as :

$$R = \max(||\{\bar{r}\}||), \tag{18}$$

with $\bar{r}_i = r_i/\widetilde{f}^\star(p_i)$. The accuracy of the Newton-Gauss algorithm is ensured by a fixed tolerance tol (if $R \leq tol = 10^{-6}$). In this illustrative example $ite = 4$ iterations were enough to converge and we can observe that the decomposition on sinus basis function is more adapted to recover the reference sinusoidal solution function.

The algorithm can also be applied to periodic signals of higher order, as in the following example, where the reference function to reconstruct is defined as :

$$\widetilde{f}(t) = \sum_{k=1}^{3} \widetilde{a}_k \sin(\widetilde{\omega}_k t + \widetilde{\phi}_k), \tag{19}$$

with $(\widetilde{a}_1, \widetilde{a}_2, \widetilde{a}_3) = (1, 2, 2)$, $(\widetilde{\omega}_1, \widetilde{\omega}_2, \widetilde{\omega}_3) = (2, 15, 3)$ and $(\widetilde{\phi}_1, \widetilde{\phi}_2, \widetilde{\phi}_3) = (\pi/6, \pi/4, \pi/3)$.
The convergence of the algorithm is illustrated in Fig. 4a, which shows a negligible residuum after 7 iterations. A comparison in time between the reference and the reconstructed function is illustrated in Fig. 4b. We observe that the superposed complex periodic signal (N=3) is well recovered.

3. Computation of VE structures under large numbers of cycles

In this section, we propose a computational procedure for VE structures subjected to large numbers of loading cycles.

3.1. Problem statements in time and L-C domains

We recall the equations associated with the problem in time and its equivalent in the L-C domain. Under the assumption of a quasi-static problem, without ageing, under small perturbations and in

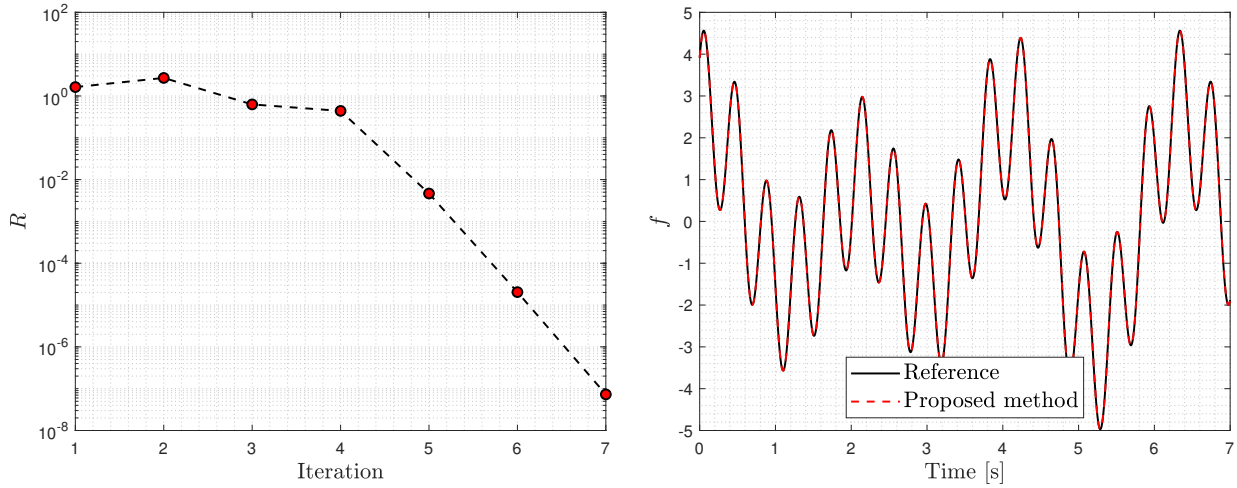

(a) Residuum of the Newton-Gauss algorithm to reconstruct the approached solution.

(b) Comparison between the reference and reconstructed function in time.

Figure 4.: Accuracy of the proposed LCT inversion for high order sinusoidal function (Eq. 19).

linear viscoelasticity, the evolution equations in time t are written as follows:

- Field equations :

$$\mathcal{P}(t) = \begin{cases} \boldsymbol{\nabla}.\boldsymbol{\sigma}(\mathbf{x},t) + \rho \boldsymbol{F}(\mathbf{x},t) = 0, \\ \boldsymbol{\varepsilon}(\mathbf{x},t) = \dfrac{1}{2}\Big(\boldsymbol{\nabla}(u(\mathbf{x},t)) + \boldsymbol{\nabla}^T(\mathbf{u}(\mathbf{x},t))\Big), \\ \boldsymbol{\sigma}(\mathbf{x},t) = \displaystyle\int_{-\infty}^{t} \mathbb{C}(\mathbf{x},t-\tau) : \dot{\varepsilon}(\mathbf{x},\tau) d\tau, \end{cases} \tag{20}$$

where $\mathbb{C}(t)$ is the fourth-order isotropic relaxation tensor :

$$\mathbb{C}(t) = 2G(t)\mathbb{I}^{\text{dev}} + 3K(t)\mathbb{I}^{\text{vol}}, \tag{21}$$

the set $(\mathbb{I}^{\text{dev}}, \mathbb{I}^{\text{vol}})$ are respectively the fourth-order deviatoric and volumetric projection tensors and (G, K) are the shear and bulk relaxation moduli expressed here as Prony series :

$$G(t) = G_\infty + \sum_{i=1}^{I} G_i e^{-t/g_i}, \tag{22}$$

$$K(t) = K_\infty + \sum_{j=1}^{J} K_j e^{-t/k_j}. \tag{23}$$

Here (G_∞, K_∞) is the set of long-term moduli, (g_i, k_j) the set of relaxation times, and (G_i, K_j) the set of weights for the shear and bulk moduli.

- Boundary conditions :

$$\mathcal{B}(t) = \begin{cases} \partial\Omega_u \cap \partial\Omega_T = \varnothing,\ \partial\Omega_u \cup \partial\Omega_T = \partial\Omega, \\ u_i(\mathbf{x},t) = u_i^d(\mathbf{x},t), \text{ on } \partial\Omega_u, \\ T_i(\mathbf{x},t) = T_i^d(\mathbf{x},t), \text{ on } \partial\Omega_T, \end{cases} \tag{24}$$

where $\partial\Omega_u$ and $\partial\Omega_T$ are respectively the regions where the boundary conditions in displacement u_i^d and the stress vector T_i^d are applied.

The mechanical time problem can be transformed via the LCT into a linear elastic problem in the L-C domain (Correspondence principle [15, 26]), such as :

- Field equations :

$$\mathcal{P}^\star(p) = \begin{cases} \boldsymbol{\nabla}.\boldsymbol{\sigma}^\star(\mathbf{x},p) + \rho\boldsymbol{F}^\star(\mathbf{x},p) = 0, \\ \boldsymbol{\varepsilon}^\star(\mathbf{x},p) = \dfrac{1}{2}\Big(\boldsymbol{\nabla}(u^\star(\mathbf{x},p)) + \boldsymbol{\nabla}^T(\mathbf{u}^\star(\mathbf{x},p))\Big), \\ \boldsymbol{\sigma}^\star(\mathbf{x},p) = \mathbb{C}^\star(\mathbf{x},p) : \boldsymbol{\varepsilon}^\star(\mathbf{x},p), \end{cases} \tag{25}$$

- Boundary conditions :

$$\mathcal{B}^\star(p) = \begin{cases} \partial\Omega_u \cap \partial\Omega_T = \varnothing,\ \partial\Omega_u \cup \partial\Omega_T = \partial\Omega, \\ u_i^\star(\mathbf{x},p) = u_i^{d\star}(\mathbf{x},p), \text{ on } \partial\Omega_u, \\ T_i^\star(\mathbf{x},p) = T_i^{d\star}(\mathbf{x},p), \text{ on } \partial\Omega_T, \end{cases} \tag{26}$$

3.2. A first structural application

The structural application considered in this Section is illustrated in Fig. 5. The 2D plane strain configuration (meshed with 10 344 linear triangular elements and 5356 nodes) has been chosen to accelerate the computation and obtain the direct reference solution under 10k cycles with a standard computer (6600U/i7, 2.60GHz/4CPU, 16GB/RAM). The reference solution computed in time domain will be compared to the solution reconstructed with the proposed method.

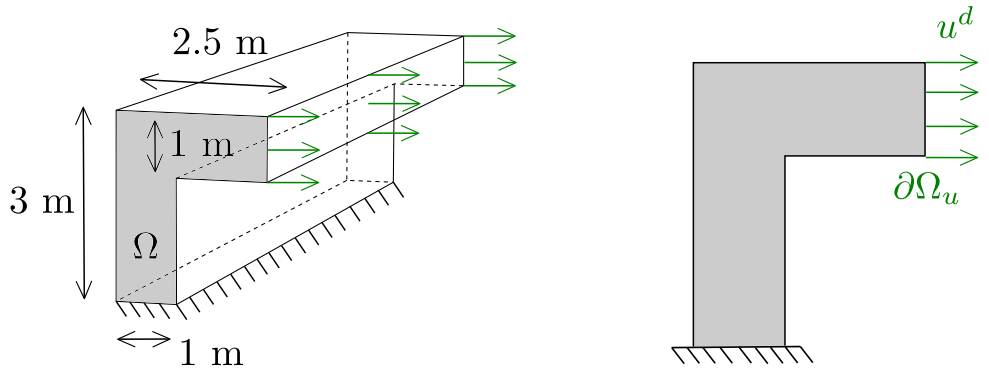

Figure 5.: VE structure under cyclic loading, 3D geometry and 2D plane strain model.

3.2.1. Signal decomposition and split computational procedure

In this application the system is loaded by a prescribed cyclic displacement (see the black curve in Fig. 6a), following the function :

$$u_1^d(\mathbf{x},t) = \widetilde{u}_1^d(\mathbf{x},t) + \widehat{u}_1^d(\mathbf{x},t), \quad \forall \mathbf{x} \in \partial\Omega_u. \tag{27}$$

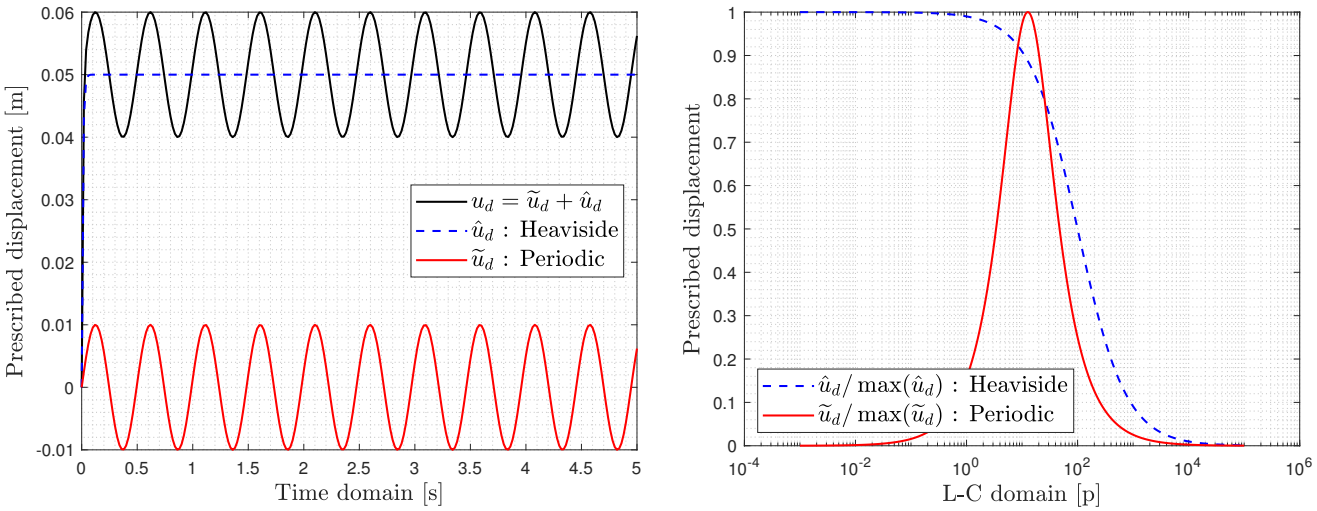

(a) Loading functions decomposition in time domain.

(b) Loading functions split in L-C domain.

Figure 6.: Decomposition of the loading signal into Heaviside and periodic parts. (a) Time domain, (b) L-C domain.

This decomposition of the loading signal is used to apply the superposition principle to cumulate the transient response due to the $\widehat{u}_1^d$ function (see the blue curves in Fig. 6a in time and in Fig. 6b in L-C domain), expressed as :

$$\widehat{u}_1^d(t) = \widehat{A}(1 - e^{-t/\widehat{\theta}}), \tag{28}$$

and the periodic response according to the sinus loading $\widetilde{u}_i^d$ (see the red curves in Fig. 6a in time and in 6b in L-C domain), such as :

$$\widetilde{u}_1^d(t) = \widetilde{A}\sin(\widetilde{\omega}t + \widetilde{\phi}), \tag{29}$$

where $\widehat{\theta} << \widetilde{\omega}$ (in mathematical sense), to approximate a Heaviside function by an exponential function in order to use a continuous function in L-C domain.

Each subproblem (transient/periodic) needs a particular LCT inversion treatment :

- transient subproblem will use the Schapery LCT inversion (see Sec. 2.1),
- periodic subproblem will employ the proposed LCT inversion method based on the sinus basis decomposition (see Sec.2.2).

In the next part we will describe step by step the proposed procedure (illustrated in Fig. 7) and compare the reconstructed solutions with the reference. The simulations are based on the parameters reported in Tab. 1 used in [27] for semi-crystalline polyamide polymer.

The sampling points p_i in the L-C domain have to be chosen. Indeed they affect directly the accuracy of the solution and their choice depends on the problem formulation and its parameters. A methodology is proposed here and as the cyclic problem is separated into two sub-problems, each case can have a different discretization. For both, we have fixed 30 sampling points distributed according to the evolution of each set of parameters : $(\widehat{K}^\star, \widehat{G}^\star, \widehat{u}^\star)$ illustrated in Fig. 8a and $(\widetilde{K}^\star, \widetilde{G}^\star, \widetilde{u}^\star)$ in Fig. 8b, which are respectively attached to each sub-problem. The methodology here is to select some points : $(p_i^{(1)}, p_i^{(2)})$ which are sufficient to represent for each case the three evolutions simultaneously.

The shear and bulk relaxation moduli in time defined by Prony series in Eq. 22,23 are expressed

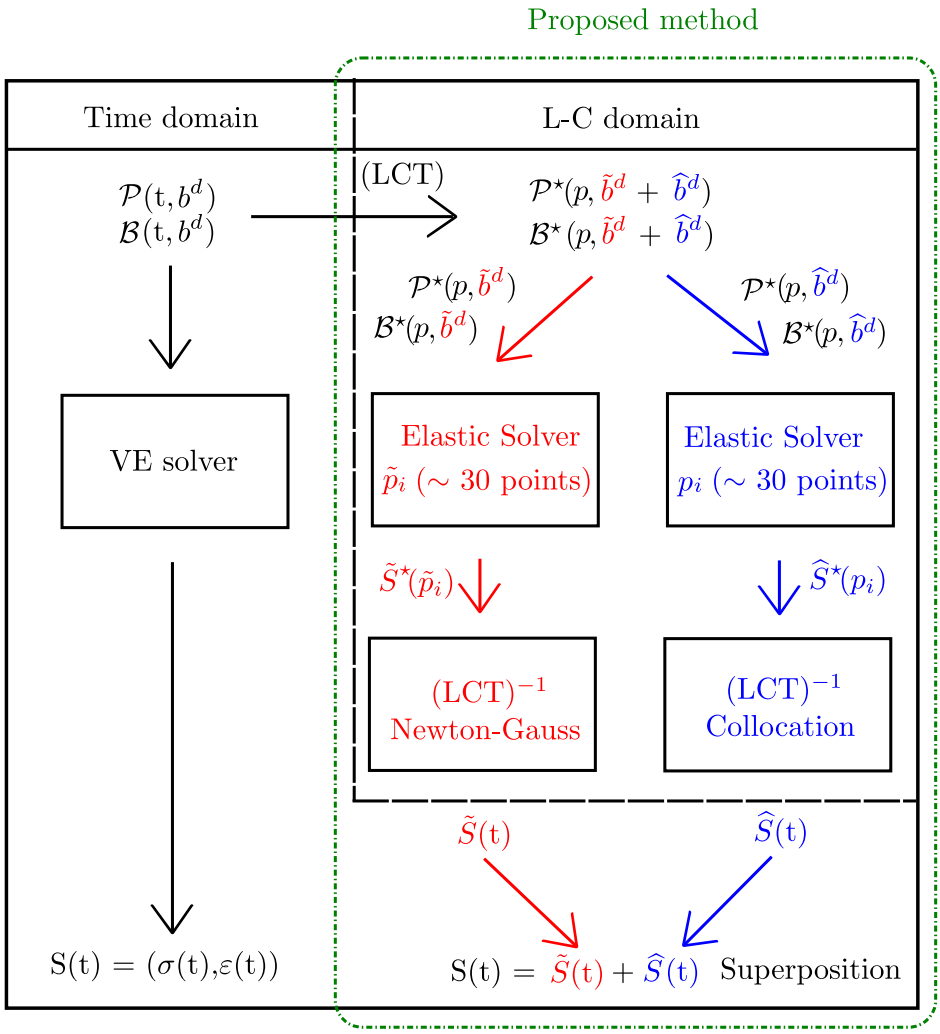

Figure 7.: FE simulation strategy of VE structure under cyclic (displacement $b_d = u^d$ or force $b_d = T^d$) loading. Left : direct time domain computation to obtain reference solution. Right : proposed procedure in L-C domain followed by split numerical inversion for LCT.

VE parameters			
Initial shear modulus	$G_0 = 1074$ MPa	Initial bulk modulus	$K_0 = 3222$ MPa
G_i (MPa)	g_i (s)	K_j (MPa)	k_j (s)
158	0.021	472	0.007
80	0.378	242	0.126
37	0.648	111	0.216
Loading parameters			
$\widehat{u}_1^d$	$\widehat{A} = 0.05$ m	$\widehat{\theta} = 0.01$	
$\widetilde{u}_1^d$	$\widetilde{A} = 0.01$ m	$\widetilde{\omega} = 4\pi$ rad/s	$\widetilde{\phi} = 0$

Table 1.: VE problem parameters [27].

according to their LCTs as :

$$G^\star(p) = G_\infty + \sum_{i=1}^{I} G_i \frac{p}{p + 1/g_i}. \tag{30}$$

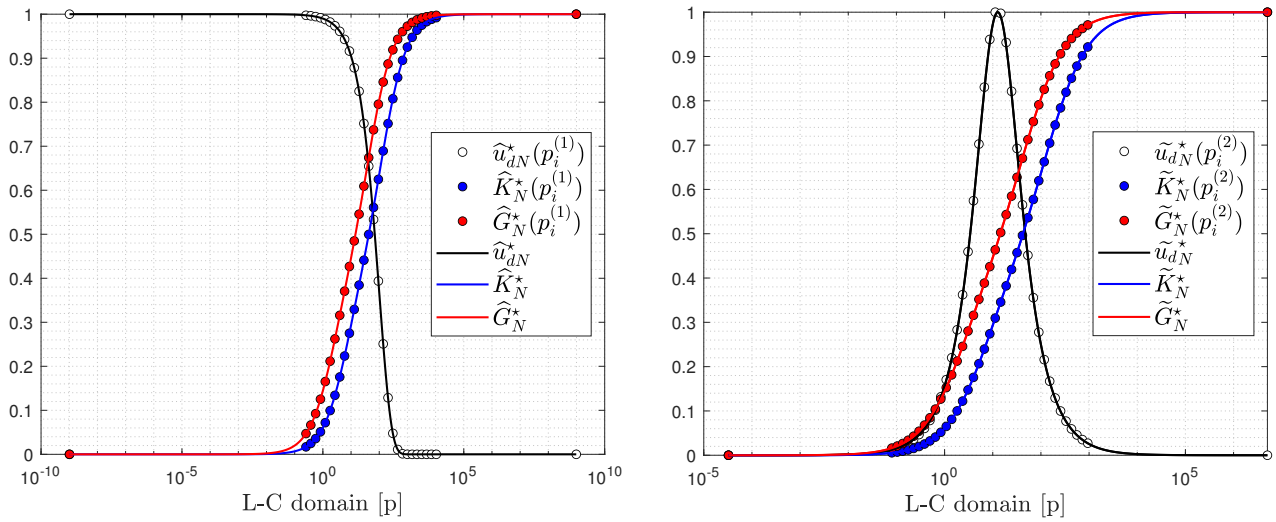

(a) Transient problem. (b) Periodic problem.

Figure 8.: Selection of the discretization points in L-C domain for (a) transient problem, (b) periodic problem.

and

$$K^\star(p) = K_\infty + \sum_{j=1}^{J} K_j \frac{p}{p + 1/k_j}, \tag{31}$$

The LCT of the transient part (Eq. 28) of the displacement is :

$$\widehat{u}_d^\star(p) = \widehat{A}\frac{p}{p + 1/\widehat{\theta}}, \tag{32}$$

and the LCT of the periodic part (Eq. 29) is :

$$\widetilde{u}_d^\star(p) = \widetilde{A}\frac{p^2}{\widetilde{\omega}^2 + p^2}\sin\widetilde{\phi} + \widetilde{A}\frac{p\widetilde{\omega}}{\widetilde{\omega}^2 + p^2}\cos\widetilde{\phi}, \tag{33}$$

Fig. 8 shows how the sampling is placed in the L-C domain. To illustrate all the parameters of each sub-problem on the same graphic, we apply on these parameters the shifted and normalized function defined as :

$$P_N^\star = \frac{P^\star - \min(P^\star)}{\max(P^\star - \min(P^\star))}, \tag{34}$$

where $P^\star$ is applied on $(K^\star, G^\star)$ moduli and for the two prescribed displacements $(\widehat{u}_d^\star, \widetilde{u}_d^\star)$.

We give hereafter guidelines regarding the assignment of sampling points, and more information is provided in Appendix B.

- Minimum and maximum points containing for each sub-problem, the spectra in the L-C domain of the shear and bulk moduli and imposed displacement. In particular for the transient response, we have to identify the A and B parameters defined as the limits in zero and infinity (see Eq. 5 and 6) for the LCT inversion using the Schapery's collocation method. In pratice, as the parameters are defined as *a priori* functions, it is straightforward to select numerically the two bounds.
- Number of sampling points. For the transient response, as explained in Section. 2.1 and illustrated in Fig. 2, the Schapery's collocation method needs a number of points respecting over- and undersampling constraints. For the sinusoidal response, the method proposed and described

in Section. 2.2 requires only a minimal number of points. In practice, this selection on sampling requires a short preliminary study as explained in Section 2 introducing the Schapery's collocation method and the proposed method.

- Positioning of the sampling between two bounds, highlighted on the regions of strong curvature. Indeed, the sampling in p_i of these functions is crucial to ensure an accurate LCT inversion, as suggested in [13]. In practice the application of a curvilinear log-linear distribution algorithm for sampling is appropriate.

3.2.2. Application to the first loading cycles

In this part, we consider the first ten cycles. The VE problem in time (Eq. 20 & 24) fully parametrized with Tab. 1 is solved first, using implicit dynamic time scheme algorithm for N-cycles ($t \in [0;5]$s, $\Delta t = 0.02$s, $N_c =\sim 10$ cycles), under u_1^d (Heaviside+periodic) displacement boundary condition (here we imposed : $T^d = 0$) as illustrated in Fig. 6a. The response constitutes the reference solution to assess the proposed method. Then the VE problem in L-C domain $(\mathcal{P}^\star, \mathcal{B}^\star)$ (see Eq. 25 & 26) is solved for the displacement boundary condition (see Eq. 32 & 33) split in two $(\widehat{u}_d, \widetilde{u}_d)$. The methodology is illustrated in Fig. 7. The full comparison (large numbers of loading cycles) will be shown in the last part, here a preliminary validation for the VE problem in time is conducted, allowing to compare each evolution (periodic/transient) independently as well as the first cycles. Numerically, the method employed to recover the periodic response function needs a starting point for the iterative resolution in each Gauss point of the structure. It was found that the choice of the starting point selected on the parameters of the imposed displacement function $(a_1^{(0)}(\gamma) = \widetilde{A}$, $\omega_1^{(0)}(\gamma) = \widetilde{\omega}$, $\phi_1^{(0)}(\gamma) = \widetilde{\phi}$, where γ represents the displacement, strain, or stress solution) yields a fast convergence of the Newton-Gauss algorithm.

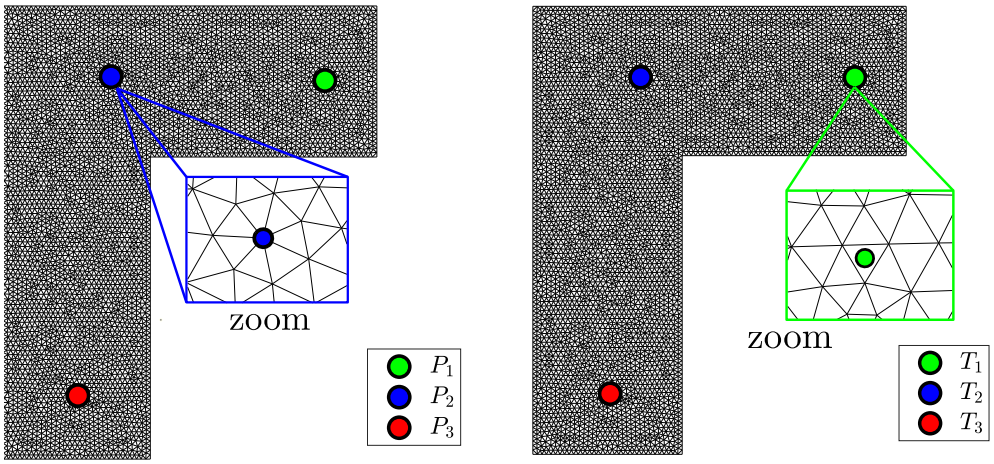

(a) Nodal points selected. (b) Gauss points selected.

Figure 9.: Points of interest selected for future comparisons between reference and proposed methods, (a) nodal points $P_{1\mapsto 3}$, (b) Gauss points $T_{1\mapsto 3}$.

Figure. 9 shows some points of interest chosen in the structure for comparison between reference solution and proposed method; there are 3 nodal points ($P_{1\mapsto 3}$, see Fig. 9a) and 3 Gauss points ($T_{1\mapsto 3}$, see Fig. 9b).

The x- and y-displacements at points $P_{1\mapsto 3}$ are plotted in Fig. 10 for the $\widehat{u}_d$ Heaviside part of the imposed displacement and in Fig. 11 for the $\widetilde{u}_d$ periodic part.

Figures. 10 and 11 show that for both problems, the recovered time evolutions of the x- and y-displacements at points $P_{1\mapsto 3}$ obtained with the proposed LCT inversion methods match perfectly the

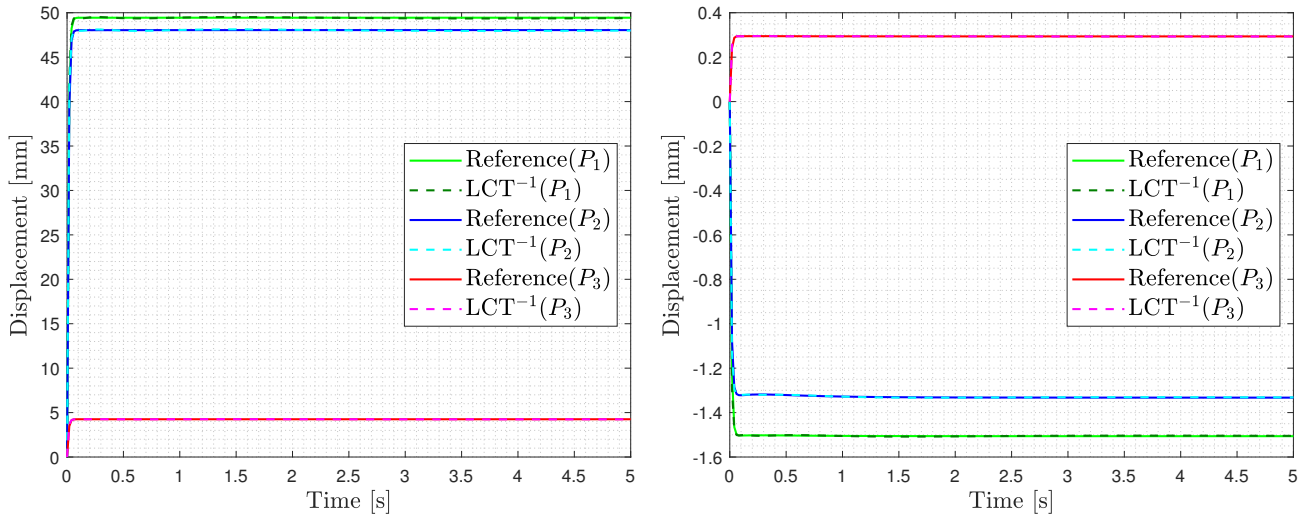

(a) x-displacement (b) y-displacement

Figure 10.: Displacements at 3 points of interest in Fig. 9a, computed with proposed method and reference solution (Heaviside boundary condition).

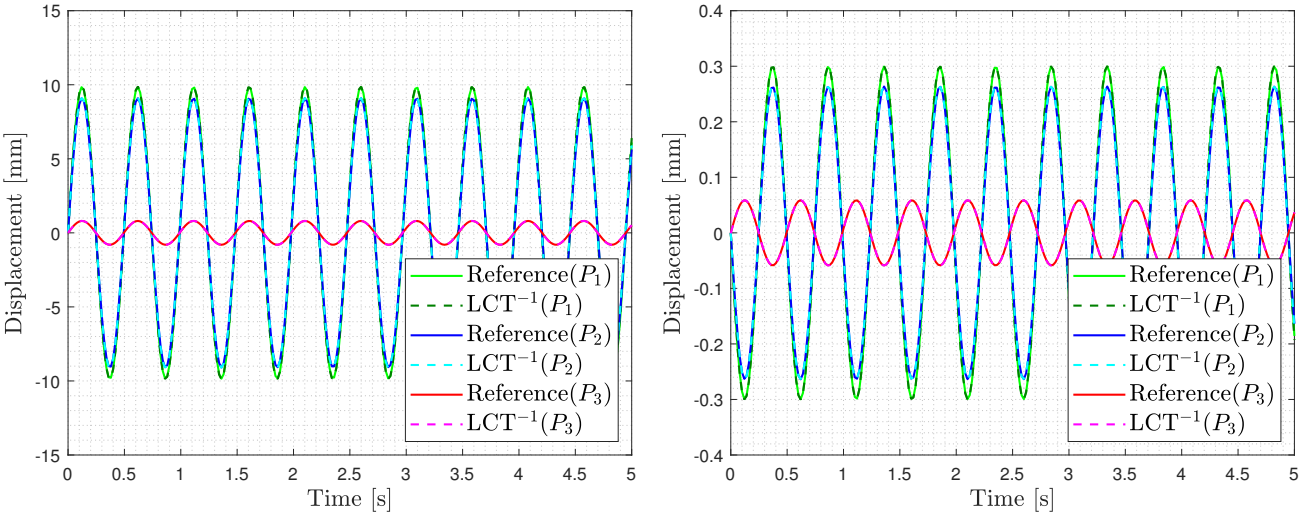

(a) x-displacement (b) y-displacement

Figure 11.: Displacements at 3 points of interest in Fig. 9a, computed with proposed method and reference solution (sinus boundary condition).

reference values obtained with direct Finite Element Analysis solved in the time.

3.2.3. Application to a large number of loading cycles

In this part, we compare the proposed method's results with the reference full calculation for a large number of cycles ($N_c = 10$k, $t \in [0; 5000]$ s, $\Delta t = 0.02$s). For this purpose, each component of the strain and stress tensors in points of interest ($T_{1 \mapsto 3}$ in Fig. 9b) is compared with the reference response in Figs. 12-14.

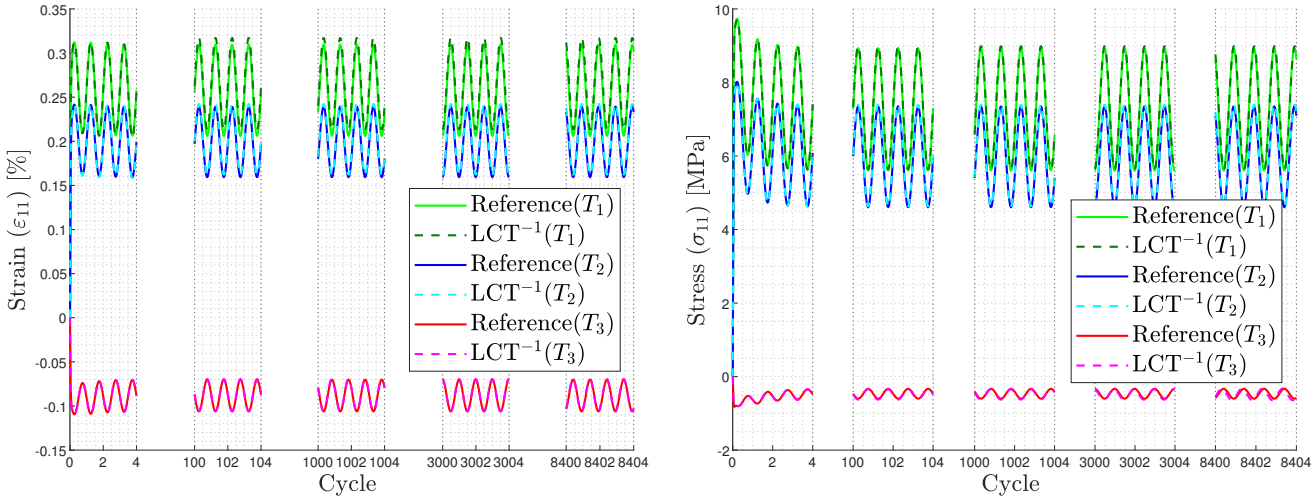

Figure 12.: VE structure under a large number of loading cycles. Comparison of strain (ε_{11}) and stress (σ_{11}) components at 3 points of interest of Fig. 9b computed with reference solution and with proposed method.

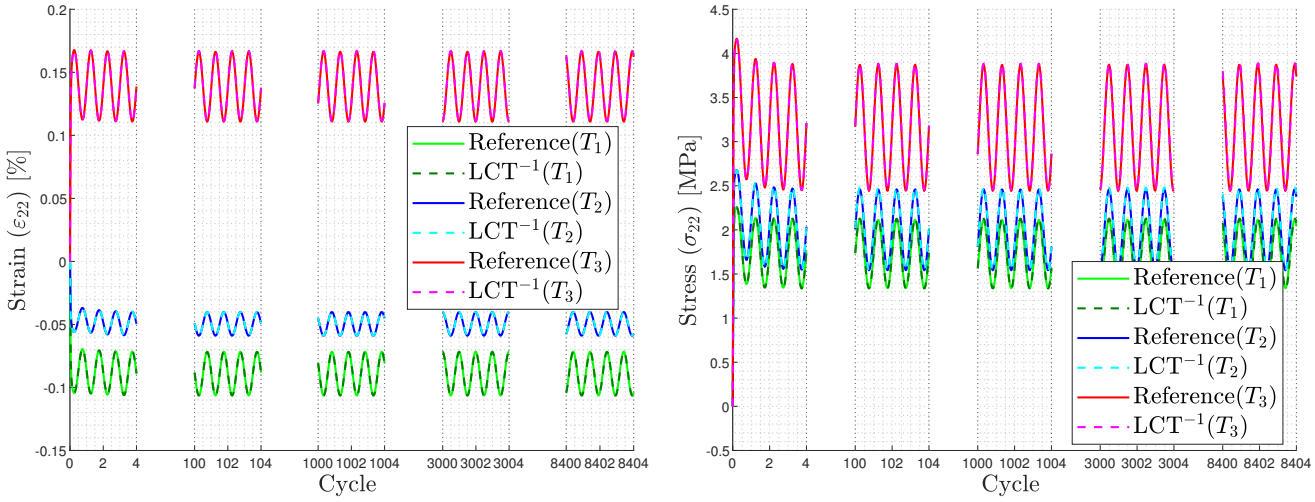

Figure 13.: VE structure under a large number of loading cycles. Comparison of strain (ε_{22}) and stress (σ_{22}) components at 3 points of interest of Fig. 9b computed with reference solution and with proposed method.

The figures show that all strain and stress components are extremely well recovered.

A second point of comparison based on a global energy indicator for the entire structure and providing a global estimation of the accuracy of the proposed method was established. The global energy indicator as a function of time is defined here as :

$$\mathrm{W(t)} = \frac{1}{V_\Omega} \int_\Omega \boldsymbol{\sigma}(\mathbf{x}, t) : \boldsymbol{\varepsilon}(\mathbf{x}, t) dV. \tag{35}$$

The comparison of W(t) obtained with the proposed method and with the reference solution is illus-

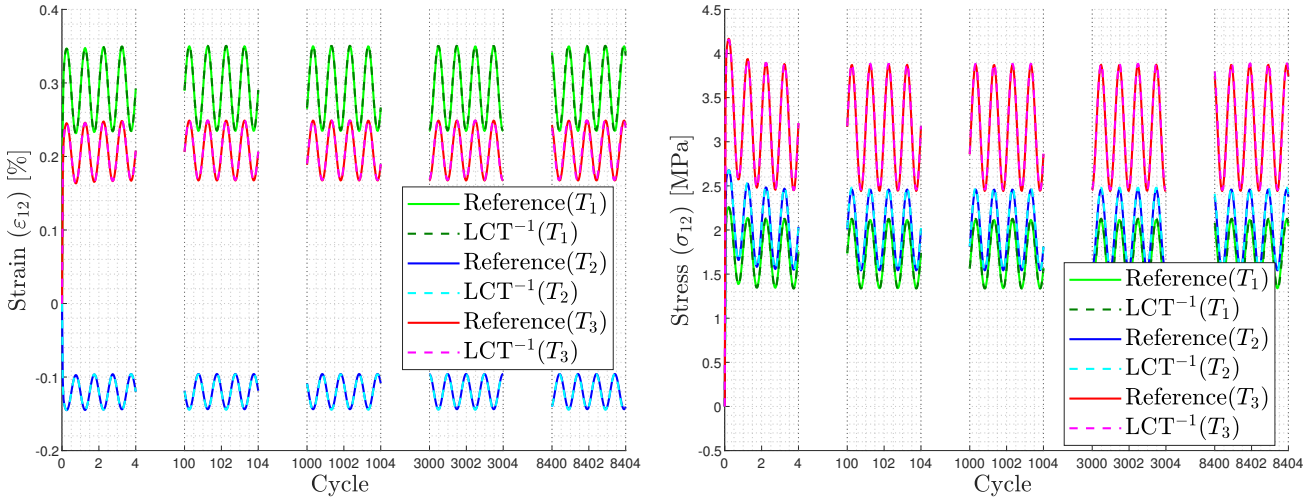

Figure 14.: VE structure under a large number of loading cycles. Comparison of strain (ε_{12}) and stress (σ_{12}) components at 3 points of interest of Fig. 9b computed with reference solution and with proposed method.

335 trated in Fig. 15a, which shows that W(t) is qualitatively well reproduced for various cycles.

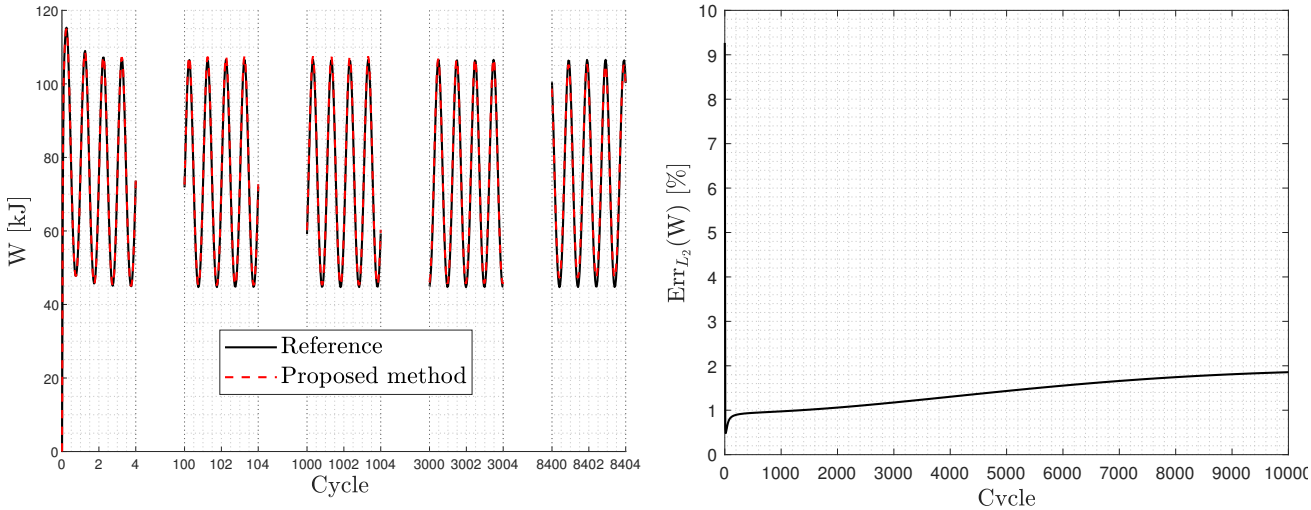

(a) Time (cycle) evolution of a global energy indicator.

(b) Time (cycle) evolution of the L_2-error on W(t).

Figure 15.: Global accuracy evaluation of proposed method against reference solution for the VE structure of Fig. 5.

336 To have a quantitative estimation, the L-2 relative error on W(t) :

337

$$\mathrm{Err}_{L_2}(W(t)) = \sqrt{\frac{\int_0^t [W^{\mathrm{Ref}}(t') - W^{\mathrm{LCT}^{-1}}(t')]^2 dt'}{\int_0^t [W^{\mathrm{Ref}}(t')]^2 dt'}} \tag{36}$$

338

339

340 was calculated. The results are plotted in Fig. 15b.

341 It is seen that the error on the global energy indicator drops rapidly, then it increases weakly with
342 the number of cycles before stabilizing. At 10k cycles, the error remains lower than 2%.

3.2.4. Computational gain

The numerical costs of the reference calculation in time and the reconstructed solutions using the proposed method based on LCT inversion are detailed in Appendix C, Table C1, including the CPU time used at each calculation step, and following the methodology scheme in Fig. 7. As for the simulation tools, Abaqus software was used for all FE calculations, while the numerical LCT inversions to reconstruct temporal responses and the post-processing were performed in Matlab.

To summarize the numerical study, the method that is proposed here and applied to the structure depicted in Figs. 5 and 9, for N_c =10k cycles, generates a relative error of L-2 norm less than 2 % in the global energy indicator for a factor gain in time of $G_T = 32$, which represents $\mathrm{T_{ref}} = 96$ hours for the reference calculation against $\mathrm{T_{pm}} = 3$ hours for the proposed method and its post-processing. It should be noted that the proposed method has a fixed computational cost of 2h30 and is independent of the number of cycles whereas the reference time calculation is a linear function of the number of cycles. Thus, without taking into account the post-processing, we can estimate by extrapolation with the number of cycles a gain factor of time between the two calculations such as :

$$G_T = \frac{\mathrm{T_{ref}}}{\mathrm{T_{pm}}}, \tag{37}$$

where T is the computational time, respectively of the reference (ref) and the proposed method (pm).

The evolution of the computational gain is illustrated in Fig. 16 and shows a great time performance for very large numbers of cycles. As discussed in the introduction in Section. 1, the computational gain will play a key role in future work.

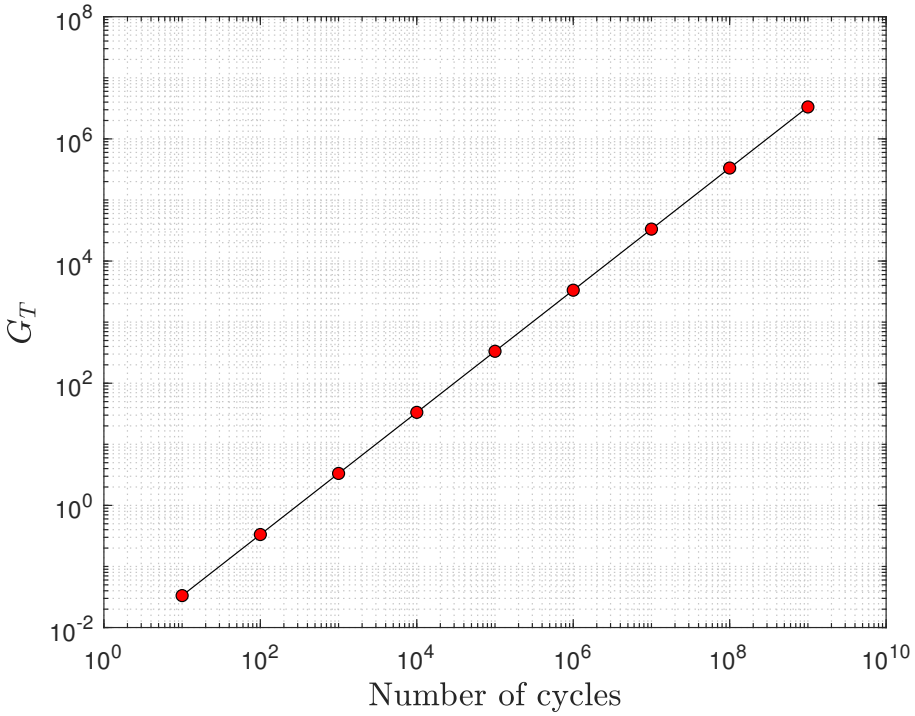

Figure 16.: Computational time gain factor.

3.3. A second structural application

In this Section, the proposed method is applied to a VE arc subjected to a cyclic force (see Fig. 17), applied to an extremity of the geometry $\partial\Omega_T$. The cyclic time history of the applied force and its decomposition are form-identical to those of the applied boundary displacement in the previous structural problem of Section 3.2; see Eqs. 27 to 29, with ($\widehat{A} = 1.10^6$ Pa, $\widetilde{A} = 1.10^5$ Pa). The force is applied vertically $T_1^d = 0$. The structure is discretized with 13 860 linear triangular elements and 7 174 nodes.

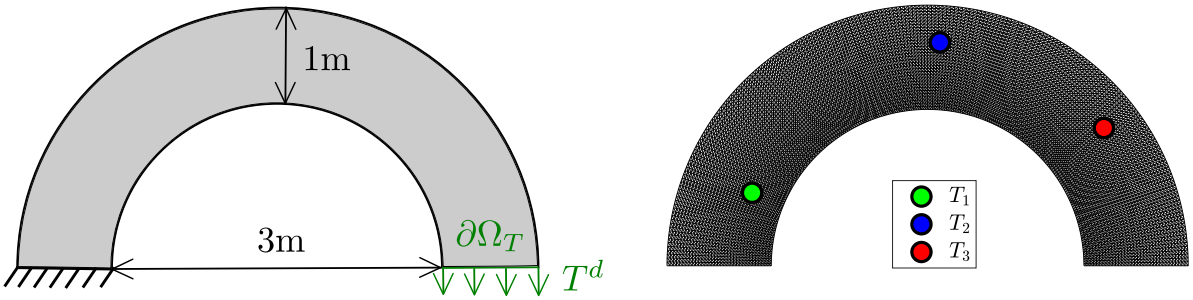

Figure 17.: VE arc under cyclic loading, 2D plane strain model and points of interest selected for future comparisons between reference solution and proposed method; 3 Gauss points ($T_{1\mapsto 3}$).

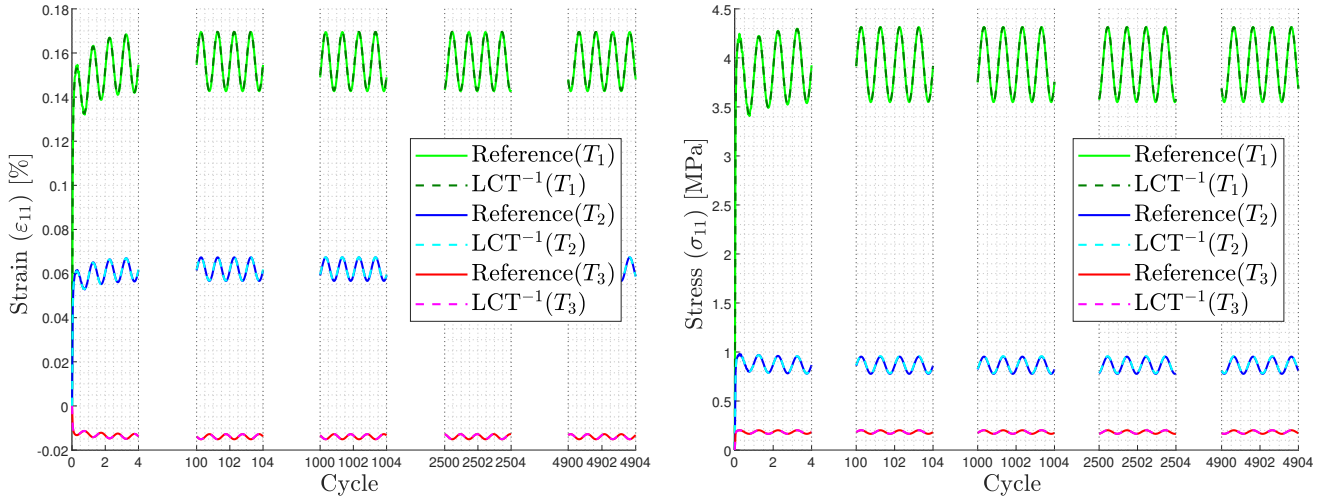

Figure 18.: VE arc under a large number of loading cycles. Comparison of strain (ε_{11}) and stress (σ_{11}) components at 3 points of interest of Fig. 17 computed with reference solution and with proposed method.

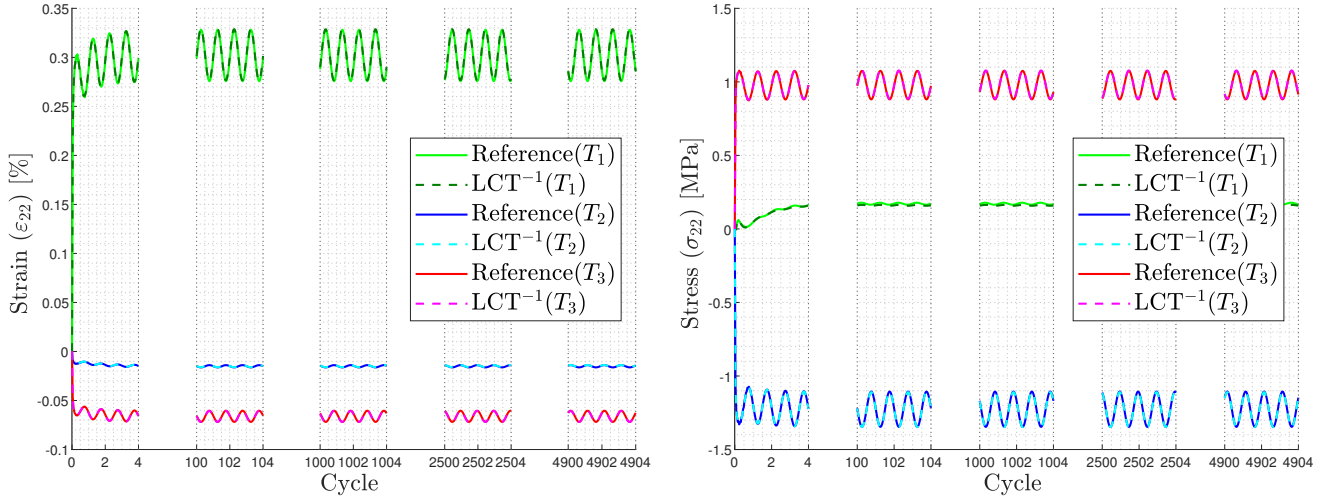

Figure 19.: VE arc under a large number of loading cycles. Comparison of strain (ε_{22}) and stress (σ_{22}) components at 3 points of interest of Fig. 17 computed with reference solution and with proposed method.

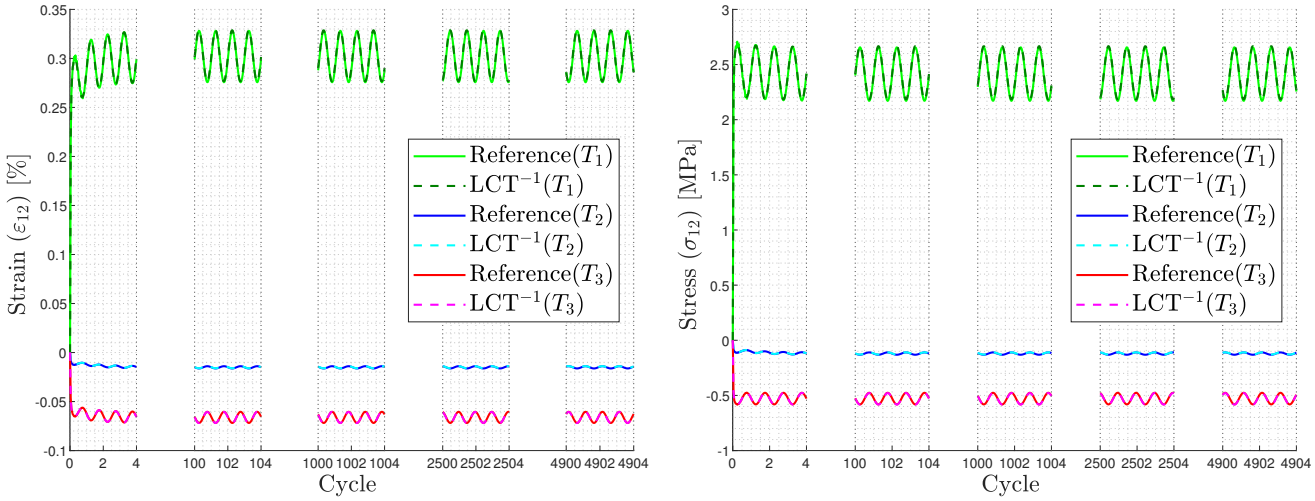

Figure 20.: VE arc under a large number of loading cycles. Comparison of strain (ε_{12}) and stress (σ_{12}) components at 3 points of interest of Fig. 17 computed with reference solution and with proposed method.

As in the previous application, a comparative study was conducted, first locally on three points (see Fig. 17), and on the entire structure with the global energy indicator (see.Eq. 35) over 5k cycles ($t \in [0; 2500]$ s). The local comparisons are shown in Figs. 18,19,20 for strain and stress components and global values in Figs. 21a,21b.

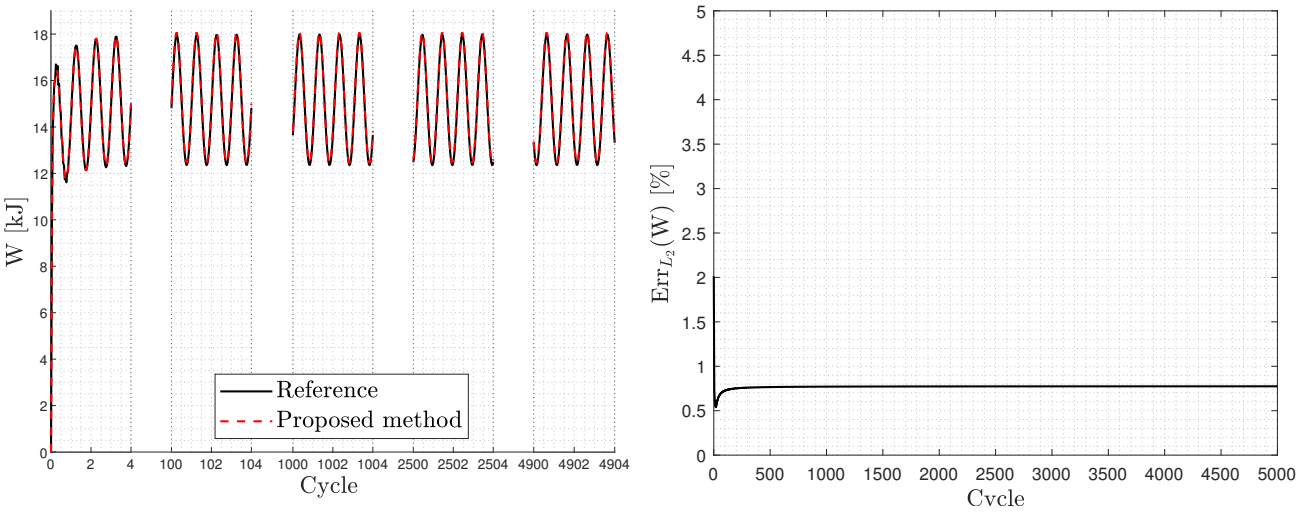

(a) Time (cycle) evolution of a global energy indicator.

(b) Time (cycle) evolution of the L_2-error on W(t).

Figure 21.: Global accuracy evaluation of proposed method against reference solution for the VE arc of Fig. 17.

Again, and similarly to the first structural application, all the local and global results show a good qualitative and quantitative reproduction of the reference solution with an error on the global energy indicator lower than 1%. The CPU time speedup factor of the proposed method as compared to the reference solution is about 16.

4. Conclusions

In this paper, a computational time reduction method for solving VE structural problems under large numbers of loading cycles was proposed. The strategy is based on an extension of the LCT method and built on a decomposition of the problem into a first transient part that can be treated numerically by Schapery's collocation method, and a second sinusoidal periodic part using a new LCT inversion method. This proposed method defines the periodic solution on a sinusoidal basis in the L-C domain and uses a Newton-Gauss algorithm enabling the LCT inversion in the time domain. The modeling and the numerical implementation of these two parts were first applied on the case of well-known 1D functions. Then, the accuracy of the proposed method was assessed on two structural problems under large numbers of cycles (10 k and 5 k cycles, respectively). A methodology as well as the comparison with reference solutions have been provided, both at local scale (displacement, strain and stress components at different points) and macroscale (global energy indicator). The results show very accurate results at local and global levels, a L-2 relative error on the global energy indicator less than 2 %. The CPU time speedup factor of the proposed method as compared to the reference solution is about 33 for the 10k cycles application.

The proposed method allows to obtain a total strain history at any location in a VE structure subjected to a large number of loading cycles. Consequently, a multiscale model combining VE computations at macroscale of the structure and complex microstructures and constitutive models at the microscale(VE matrix with porosity and VE-VP weak spots), as discussed in the introduction (Section 1) is now being developed. The (very) low computational cost of the procedure proposed in the present article will play a fundamental role in rendering the multiscale model affordable for the simulation of high cycle fatigue of polymer solids and structures.

Declaration of competing interest

The authors declare that they have no known competing financial interests or personal relationships that could have appeared to influence the work reported in this paper.

Acknowledgments

The present work was conducted and funded within the framework of the European Union's Horizon 2020 research and innovation programme for the project "Multi-scale Optimisation for Additive Manufacturing of fatigue resistant shock-absorbing MetaMaterials (MOAMMM)", grant agreement No. 862015, of the H2020-EU.1.2.1. - FET OpenProgramme.

References

[1] P. Parandoush and D. Lin, "A review on additive manufacturing of polymer-fiber composites," *Composite Structures*, vol. 182, pp. 36–53, 2017.

[2] L. Adam, O. Lietaer, S. Mathieu, and I. Doghri, "Numerical simulation of additive manufacturing of polymers and polymer-based composites, chapter in "Structure and properties of additive manufactured polymer components", K. Friedrich and R. Walter (Editors)," pp. ISBN: 978–0–12–819535–2., 2020.

[3] M. R. Gudimetla and I. Doghri, "A finite strain thermodynamically-based constitutive framework coupling viscoelasticity and viscoplasticity with application to glassy polymers," *International Journal of Plasticity*, vol. 98, pp. 197–216, 2017.

[4] J. S. Kim and A. H. Muliana, "A time-integration method for the viscoelastic–viscoplastic analyses of polymers and finite element implementation," *International journal for numerical methods in engineering*, vol. 79, no. 5, pp. 550–575, 2009.

[5] S. Haouala and I. Doghri, "Modeling and algorithms for two-scale time homogenization of viscoelastic-viscoplastic solids under large numbers of cycles," *International Journal of Plasticity*, vol. 70, pp. 98–125, 2015.

[6] A. Krairi, I. Doghri, and G. Robert, "Multiscale high cycle fatigue models for neat and short fiber reinforced thermoplastic polymers," *International Journal of Fatigue*, vol. 92, pp. 179–192, 2016.

[7] J. C. Simo and T. J. Hughes, *Computational inelasticity*, vol. 7. Springer Science & Business Media, 2006.

[8] M. Hammoud, M. Beringhier, and J.-C. Grandidier, "A reduced simulation applied to the viscoelastic fatigue of polymers," *Comptes Rendus Mécanique*, vol. 342, no. 12, pp. 671–691, 2014.

[9] P. Zerbe, B. Schneider, and M. Kaliske, "Viscoelastic-viscoplastic-damage modeling of thermoplastics under long-term cyclic loading," *PAMM*, vol. 16, no. 1, pp. 413–414, 2016.

[10] J. R. Carson, "On a general expansion theorem for the transient oscillations of a connected system," *Physical Review*, vol. 10, no. 3, p. 217, 1917.

[11] J. R. Carson, "Electric circuit theory and the operational calculus," *The Bell System Technical Journal*, vol. 5, no. 2, pp. 336–384, 1926.

[12] C. Friebel, I. Doghri, and V. Legat, "General mean-field homogenization schemes for viscoelastic composites containing multiple phases of coated inclusions," *International journal of solids and structures*, vol. 43, no. 9, pp. 2513–2541, 2006.

[13] M. Lévesque, M. D. Gilchrist, N. Bouleau, K. Derrien, and D. Baptiste, "Numerical inversion of the Laplace-Carson transform applied to homogenization of randomly reinforced linear viscoelastic media," *Computational mechanics*, vol. 40, no. 4, pp. 771–789, 2007.

[14] A. Rekik and R. Brenner, "Optimization of the collocation inversion method for the linear viscoelastic homogenization," *Mechanics Research Communications*, vol. 38, no. 4, pp. 305–308, 2011.

[15] J. Mandel, *Cours de mécanique des milieux continus*, vol. I and II. Gauthier-Villars, 1966/re-edited 1994, J. Gabay.

[16] J. Abate and W. Whitt, "A unified framework for numerically inverting laplace transforms," *INFORMS Journal on Computing*, vol. 18, no. 4, pp. 408–421, 2006.

[17] H. Dubner and J. Abate, "Numerical inversion of Laplace transforms by relating them to the finite fourier cosine transform," *Journal of the ACM (JACM)*, vol. 15, no. 1, pp. 115–123, 1968.

[18] J. Abate and W. Whitt, "The Fourier-series method for inverting transforms of probability distributions," *Queueing systems*, vol. 10, no. 1, pp. 5–87, 1992.

[19] D. P. Gaver Jr, "Observing stochastic processes, and approximate transform inversion," *Operations Research*, vol. 14, no. 3, pp. 444–459, 1966.

[20] H. Stehfest, "Algorithm 368: Numerical inversion of Laplace transforms [d5]," *Communications of the ACM*, vol. 13, no. 1, pp. 47–49, 1970.

[21] C. Wellekens, "Generalisation of vlach's method for the numerical inversion of the laplace transform," *Electronics Letters*, vol. 6, no. 23, pp. 742–744, 1970.

[22] R. Schapery, "A method of viscoelastic stress analysis using elastic solutions," *Journal of the Franklin Institute*, vol. 279, no. 4, pp. 268–289, 1965.

[23] T. L. Cost and E. B. Becker, "A multidata method of approximate laplace transform inversion," *International journal for numerical methods in engineering*, vol. 2, no. 2, pp. 207–219, 1970.

[24] M. Lévesque, *Modélisation du comportement mécanique de matériaux composites viscoélastiques non*

linéaires par une approche d'homogénéisation. PhD thesis, PhD Thesis, Paris, ENSAM, 2004.

[25] I. Viktorova, B. Dandurand, S. Alekseeva, and M. Fronya, "Modeling the creep of polymer-based nanocomposites by using an alternative nonlinear optimization approach," *Mechanics of Composite Materials*, vol. 48, no. 6, pp. 693–704, 2013.

[26] W. N. Findley, J. S. Lai, and K. Onaran, *Creep and relaxation of nonlinear viscoelastic materials - With an introduction to Linear Viscoelasticity.* Dover Publications, New York, 1989.

[27] E. Baquet, *Modélisation thermomécanique visco-hyperélastique du comportement d'un polymère semi-cristallin: application au cas d'une matrice polyamide 6.6.* PhD thesis, École Nationale Supérieure des Mines de Paris, 2011.

Appendix A. Dependency of the LCT inversion methods on the number of sampling points

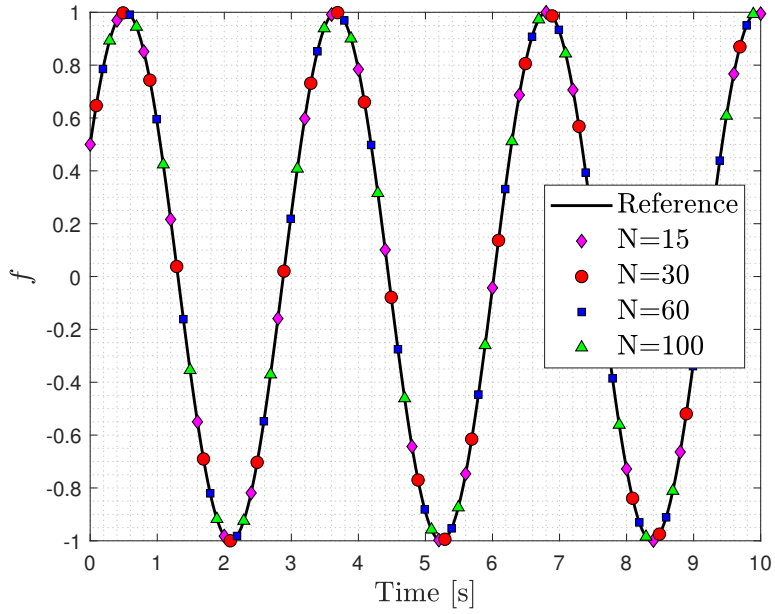

(a) Reconstruction of the sinusoidal function of Eq. 16 with the proposed method. Dependence on the number of sampling points.

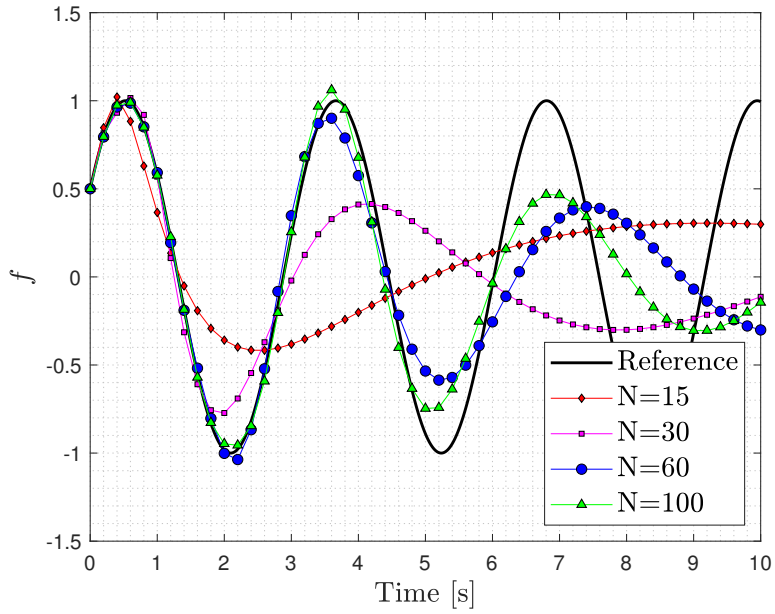

(b) Reconstruction of the sinusoidal function of Eq. 16 with Schapery's collocation method. Dependence on the number of sampling points.

Figure A1.: Dependence of the two reconstruction methods on the number of sampling points for the sinusoidal function of Eq. 16.

Appendix B. Sampling method

In this appendix, $\widetilde{K}^\star$ is a well-known function in the L-C domain, which is illustrated in Fig. B1a as a function of the L-C variable p. The first task is to find the minimum and maximum values of the sampling points, p_{min} and p_{max}. There are two issues here. First, the $[p_{min}, p_{max}]$ interval must be able to encompass the entire range of $\widetilde{K}^\star$(p). Second, the interval should not be unnecessarily large as to not waste computing time on too many sampling points where $\widetilde{K}^\star$(p) is a horizontal line. In order to achieve these two objectives, the following procedure is adopted.

Initially, far apart estimates of p_{min} and p_{max} are found. Then, different filters are applied in order to find closer estimates. The first considers the area under the $\widetilde{K}^\star$(p) curve. The second filter is based on normalized values of the first derivative of $\widetilde{K}^\star$(p). And if $\widetilde{K}^\star$(p) is not the L-C transform of a sinusoidal time function, then a third filter is applied, based on the second derivative of $\widetilde{K}^\star$(p).

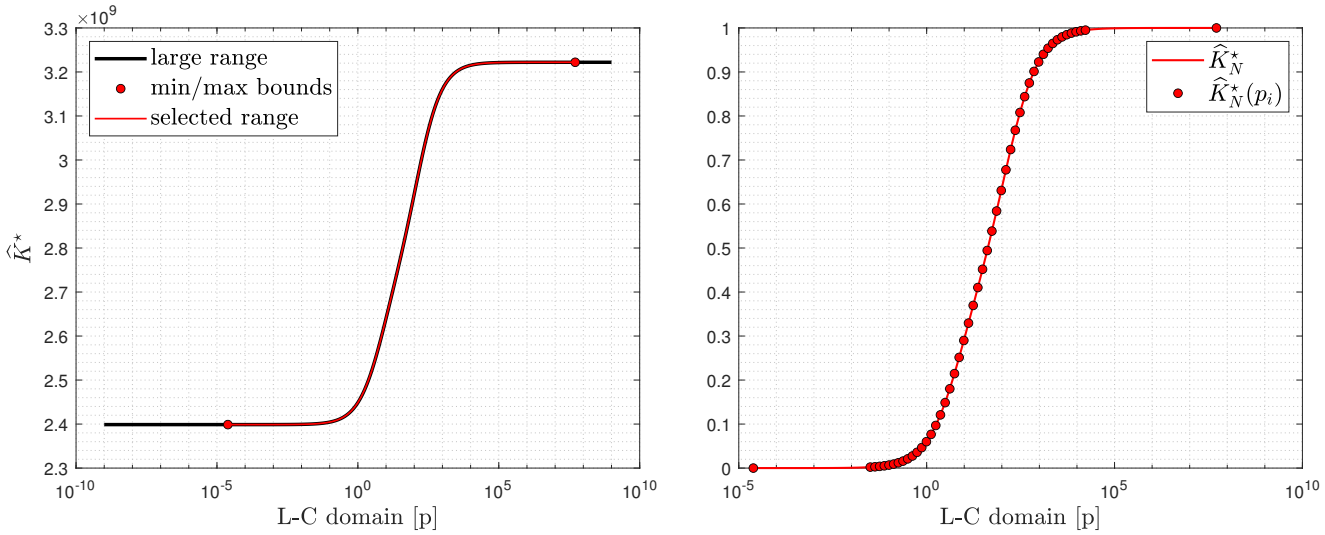

(a) Selection of the bounds and the range of $K^\star$.

(b) Sampling on the selected range.

Figure B1.: Numerical sampling selection.

Once the values of p_{min} and p_{max} have been found, the sampling points are chosen according to the following method. First, $K^\star$(p) is normalized as explained in Eq. 34. We thus obtain $\widetilde{K}^\star_N(p)$ illustrated in Fig. B1b. Next, a curvilinear sampling algorithm is applied. The main idea behind it is to divide the area under the curve $\widetilde{K}^\star_N(p)$ between p_{min} and p_{max} into a finite number of subdomains (typically, around 30) having the same area.

A final issue concerns the fact that when solving a structural VE problem under cyclic loadings, there are several known functions $\widetilde{K}^\star(p)$. Indeed, we have the L-C transforms of the time dependent bulk and shear moduli, and those of the boundary conditions corresponding to each one of the two structural sub-problems (transient and periodic). For the example problem studied in Section. 3.2, these are given by equations 30 to 33. The above procedure is applied to each of these known functions. Next, for each one of the two structural sub-problems considered independently :

(i) the smallest values among the p_{min} values is found;
(ii) the largest value among the p_{max} values is determined;
(iii) all the sampling points are arranged in ascending order;
(iv) the corresponding elastic problems are solved in the L-C domain for each sampling point.

Appendix C. Computational time comparison

Reference solution	Dependence on the number of cycles	Final time $\sim$ 4 days
VE solver :		Total time $\sim$ 3.5 days
Time domain		Cumulative time = 300 k s
	time for one t_i increment	time $\leftarrow$ 0.6 s
	time for one cycle ($\Delta t = 0.02$s $\mapsto$ 25 steps/cycle)	time $\leftarrow$ 30 s
	time for 10k cycles	time $\leftarrow$ time x 10k
Others :	Post-treatment (data extraction)	Total time $<$ 6h

Proposed method	Independence from the number of cycles	Final time $<$ 3h
Elastic (linear) solver :		Total time = 1 min
L-C domain		Cumulative time = 1 min
	time for one discrete p_i point	time $\leftarrow$ 0.8 s
	for $N_{p_i} = 30$ discrete points	time $\leftarrow$ time x 30
	for 2 boundary displacement functions	time $\leftarrow$ time x 2
LCT inversion :		Total time $<$ 2h30
Schapery's collocation method		Cumulative time = 30 min
	Calculation	time $\leftarrow$ 0.027 s
	for $N_e(\sim 10k)$ element	time $\leftarrow$ time x N_e
	for components of fields $(\boldsymbol{u}, \boldsymbol{\varepsilon})$	time $\leftarrow$ time x 6
LCT inversion for sinusoidal function		Cumulative time $<$ 1h30
	Calculation for one iteration	time $\leftarrow$ 0.083 s
	for $N_{ng} < 10$ (Newton-Gauss) iteration	time $\leftarrow$ time x 10
	for $N_e(\sim 10k)$ elements	time $\leftarrow$ time x N_e
	for components of fields $(\boldsymbol{u}, \boldsymbol{\varepsilon})$	time $\leftarrow$ time x 6
Others :	Post-treatment	Total time $<$ 30 min

Table C1.: Computational time details for the structural VE problem of Figs. 5 and 9.